Geophysical Research Letters

RESEARCH LETTER
10.1029/2018GL077976

Special Section:
Cassini's Final Year: Science Highlights and Discoveries

An SLS5 Longitude System Based on the Rotational Modulation of Saturn Radio Emissions

S.-Y. Ye[1], G. Fischer[2], W. S. Kurth[1], J. D. Menietti[1], and D. A. Gurnett[1]

[1]Department of Physics and Astronomy, The University of Iowa, Iowa City, IA, USA, [2]Institute for Space Research, Austrian Academy of Sciences, Graz, Austria

Abstract Despite the axisymmetry of Saturn's internal field, Saturn radio emissions like Saturn kilometric radiation (SKR) are modulated due to planetary rotation. With the completion of Cassini mission in September 2017, we now have around 14 years of observation of Saturn radio emissions, roughly from southern solstice to northern solstice. In this study, we extend the SLS4 longitude system to the end of the Cassini mission using a phase tracing method. The new Saturn longitude system (SLS5) organizes the observed SKR maxima around 0° subsolar longitude in both northern and southern hemispheres and can be used to organize other phenomena observed in Saturn's magnetosphere, for example, hot plasma injection events. SKR is modulated like a clock when the main source on the morning side is visible. To convert the observed phase to the clock phase, the phase of the morning side source, we also define a second longitude system SLS5*, which takes the spacecraft position into account based on a simple visibility model.

Plain Language Summary A new Saturn longitude system is defined based on the modulation phase of Saturn radio emissions, which can be used to organize other magnetospheric phenomena observed by Cassini at Saturn.

Key Points:
- Saturn's radio emissions are modulated at periods close to the planet's rotation period
- The modulation periods display hemispherical asymmetry and seasonal variation
- A new longitude system is defined based on the modulation phase of SKR

Supporting Information:
- Supporting Information S1
- Data Set S1

Correspondence to:
S.-Y. Ye,
shengyi-ye@uiowa.edu

Citation:
Ye, S.-Y., Fischer, G., Kurth, W. S., Menietti, J. D., & Gurnett, D. A. (2018). An SLS5 longitude system based on the rotational modulation of Saturn radio emissions. *Geophysical Research Letters*, *45*, 7297–7305. https://doi.org/10.1029/2018GL077976

Received 17 MAR 2018
Accepted 16 JUL 2018
Accepted article online 24 JUL 2018
Published online 8 AUG 2018
Corrected 10 SEP 2018

This article was corrected on 10 SEP 2018. See the end of the full text for details.

1. Introduction

Despite the fact that Saturn's internal magnetic field is highly symmetric with respect to its rotational axis (Burton et al., 2010), rotational modulation has been observed in Saturn radio emissions, magnetic field perturbations, charged particles, energetic neutrals, and motions of the plasma sheet, auroral oval, and magnetopause (Desch & Kaiser, 1981; Espinosa & Dougherty, 2000; Espinosa et al., 2003; Gurnett et al., 2007; Carbary et al., 2007; Paranicas et al., 2005; Andrews et al., 2008; Andrews, Coates et al., 2010; Andrews et al., 2011; Clarke, Andrews, Arridge et al., 2010; Clarke, Andrews, Coates et al., 2010; Nichols et al., 2010; Khurana et al., 2009; Provan et al., 2009, 2011; Carbary & Mitchell, 2013, and references therein; Carbary et al., 2017). A period very close to the modulation period of Saturn kilometric radiation (SKR) was originally adopted by the IAU as the rotation period of Saturn (10.656 hr) due to the lack of a trackable solid surface on the gas giant. It was later found through Ulysses radio wave observation that the modulation period of SKR changed by 1% over the time scale of years (Galopeau & Lecacheux, 2000; Lecacheux et al., 1997), indicating that the SKR period is not the real planetary rotation period (Gurnett et al., 2005). Cassini observations revealed that there is not just one but two different periods in the modulations of radio emissions and magnetic field perturbations, one associated with the northern hemisphere and the other associated with the southern hemisphere (Andrews, Cowley et al., 2010; Gurnett, Lecacheux et al., 2009; Gurnett, Persoon et al., 2009; Kurth et al., 2008; Provan et al., 2014; Ye et al., 2010). The hemispheric asymmetry may arise from different solar illumination in the two polar regions, which leads to different strength of the rotating field-aligned currents (Hunt et al., 2014, 2015). Gurnett et al. (2010) showed that the rotational modulations of SKR in the two hemispheres are subject to seasonal variation, and the two periods started to converge around the vernal equinox of Saturn in 2009. It was predicted that the two periods would cross near the vernal equinox. Afterward, the northern hemisphere would rotate at the same period as the southern hemisphere did before equinox. However, the two periods crossed each other briefly in late 2009 and started to oscillate around 10.7 hr for four years after equinox (Fischer et al., 2014, 2015), before the northern hemisphere finally slowed down toward the end of mission (Ye et al., 2016). Similar developments were also observed in magnetic field perturbations (Andrews et al., 2012; Cowley & Provan, 2016; Provan et al., 2015; Provan et al., 2018).

In this paper, we define two new Saturn longitude systems (SLSs), SLS5 and SLS5*, based on the modulation phase of SKR. We will first briefly review the previous versions of the SLS. Then we will describe the

methodology used to define SLS5 in detail. In the discussion, we will compare the new longitude system with the previous version, SLS4, for time intervals when both systems are valid.

1.1. Previous Saturn Longitude Systems

The original SLS was defined based on the SKR modulation period (10.656 hr) determined from Voyager observations (Davies et al., 1996; Seidelmann et al., 2002). After Cassini arrived at Saturn, a new longitude system was defined (SLS2) and then updated (SLS3) based on the variable period of SKR (Kurth et al., 2007, 2008). A phase tracing technique was used to track the drifting phases of SKR peaks (relative to an arbitrarily chosen guide period) as a function of time. The phase drift function was then used to correct the zeroth-order longitude defined based on the fixed guide period. The resulting longitude system is such that the SKR intensity peaks occur at 100° longitude, following the convention from Voyager studies. SLS2 is valid from 1 January 2004 to 28 August 2006, and SLS3 is valid from 1 January 2004 to 10 August 2007.

Gurnett et al. (2011) extended the longitude system to just past the August 2009 equinox, adding a separate longitude system for the northern hemisphere. Instead of tracing the SKR maximum on a phase diagram, which would introduce too much background noise, they used a narrowband tracking filter, which can separately track the modulation signals in the two hemispheres, to define the SKR-based longitude systems, one for the northern hemisphere (SLS4-N) and one for the southern hemisphere (SLS4-S). Comparison between SLS3 (only defined for the southern hemisphere) and SLS4-S showed that the two longitude systems are in reasonably good agreement during their valid intervals. The deviation between the two systems can be as large as 45°, most likely due to the polynomial expansion of the phase function used by Kurth et al. (2008). Lamy (2011) also defined phase systems for both hemispheres (2004–2010) based on the variable periods of the northern and southern SKR, the power of which was separated according to circular polarization. More recently, Lamy (2017) extended the analysis to the end of the Cassini mission.

1.2. Methodology

The process we used to define the new longitude system (SLS5) is similar to that described in Gurnett et al. (2011). Instead of the narrowband tracking filter analysis used by Gurnett et al. (2011), we developed a new method to determine the rotation rates of SKR. To do that, we have to first separate the northern and southern SKR power by looking at the polarization sense. SKR is emitted mainly as R-X mode by the unstable electron population precipitating along the auroral field lines via the so-called cyclotron maser instability (Wu & Lee, 1979). The real polarization as observed by Cassini is determined by the magnetoionic mode and the emission angle with respect to the magnetic field at the source region (Fischer et al., 2009; Lamy et al., 2010; Menietti et al., 2011). So, to Cassini, SKR would appear to be right-hand polarized in the northern hemisphere and left-hand polarized in the southern hemisphere. Based on the three-antenna and two-antenna measurements of the RPWS High Frequency Receiver (Cecconi & Zarka, 2005), the polarization of SKR can be derived and can be used to attribute the observed SKR power to either the southern (circular polarization degree $v > 0.5$) or the northern ($v < -0.5$) hemisphere. The separated SKR powers are then integrated over the frequency interval (80–500 kHz) and averaged within 10-min windows. For observations above 10° latitude, we do not separate by polarization; instead, we attribute the total SKR power to the hemisphere Cassini was in. For the period after 1 December 2016, we separated SKR power only by latitude, due to uncertainty in the polarization measurement of SKR when Cassini was close to Saturn (the assumption of Saturn center as the source of SKR was not good any more). To eliminate the distance effect (dependence of SKR power on the radial distance of observation), SKR power time series are distance-normalized by a division by the average SKR intensity over about one Saturn rotation. Before the spectrum analysis, the normalized SKR intensities are then multiplied by a Hanning window weighting function to reduce the sideband effects (Priestly, 1981).

The Least-Squares Spectral Analysis (LSSA), also known as Lomb-Scargle analysis, is a method of estimating the frequency spectrum of a time series (Lomb, 1976; Scargle, 1982). The LSSA is better suited for time series with data gaps than the Fourier transform. SKR is mainly modulated like a clock (with weaker rotating components—see end of this section), which means that the timing of the intensification is generally

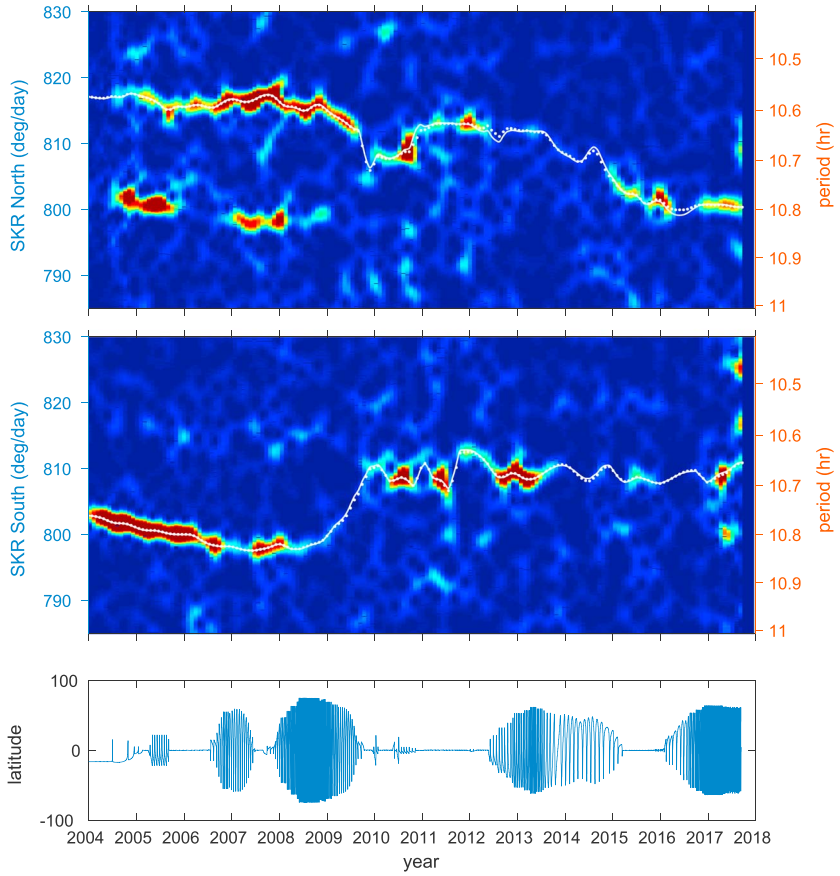

Figure 1. Rotational modulation spectrograms for SKR from the (top panel) northern and (middle panel) southern hemispheres. The spectrograms show normalized modulation power (calculated using the Least-Squares Spectral Analysis) as a function of rotation rate and time. The white dotted lines show the automatically traced rotation rates (zeroth order) of north/south SKR. The white solid lines are corrected SKR rotational modulation rates (based on the zeroth-order rates and corrected by the phase drifts traced in Figure 2). The latitude of Cassini is shown in the bottom panel.

independent of the observer's local time (Warwick et al., 1981). So we used the subsolar longitude (ωt) to organize the normalized SKR powers within a 240-day time window, assuming a rotational modulation rate ω. We also tried to organize SKR powers with respect to the subspacecraft longitude, but the resulting modulation signals were weaker compared to the organization by subsolar longitude. For each ω within the range of 790–830°/day, we fit the normalized SKR powers to a sinusoidal function of the subsolar longitude (ωt), from which we get the peak-to-peak power as a function of ω. The 240-day time window is shifted forward in 30-day steps, and the same process is repeated for each step. The resulting rotational modulation spectra are displayed as modulation spectrograms in Figure 1 (top two panels, for northern and southern SKR, respectively). The color code of the spectrograms shows the modulation power (peak-to-peak power of the sinusoidal fits), with red indicating strong modulation and blue no modulation. The bottom panel shows the latitude of Cassini.

The white dotted lines in the top and middle panels of Figure 1 are automatically traced northern and southern SKR modulation rates. About 817 and 803°/day were given as initial guesses for the northern and southern SKR rates at the beginning of 2004, and the following modulation spectra are window weighted around the peak found in the previous spectrum before we apply the peak finding algorithm. In this way big jumps in the rotation rate tracing can be avoided. The tracing results show good agreement with the intense modulation signals (red and yellow) in the modulation spectrograms and previous tracings by Gurnett et al. (2011) and Fischer et al. (2015). These zeroth-order rotation rates are integrated over time to give the zeroth-order longitudes for northern and southern hemispheres $\lambda_0 = \int \omega_0 dt$. These longitudes are then based on the time-variable zeroth-order rotation rates of Figure 1.

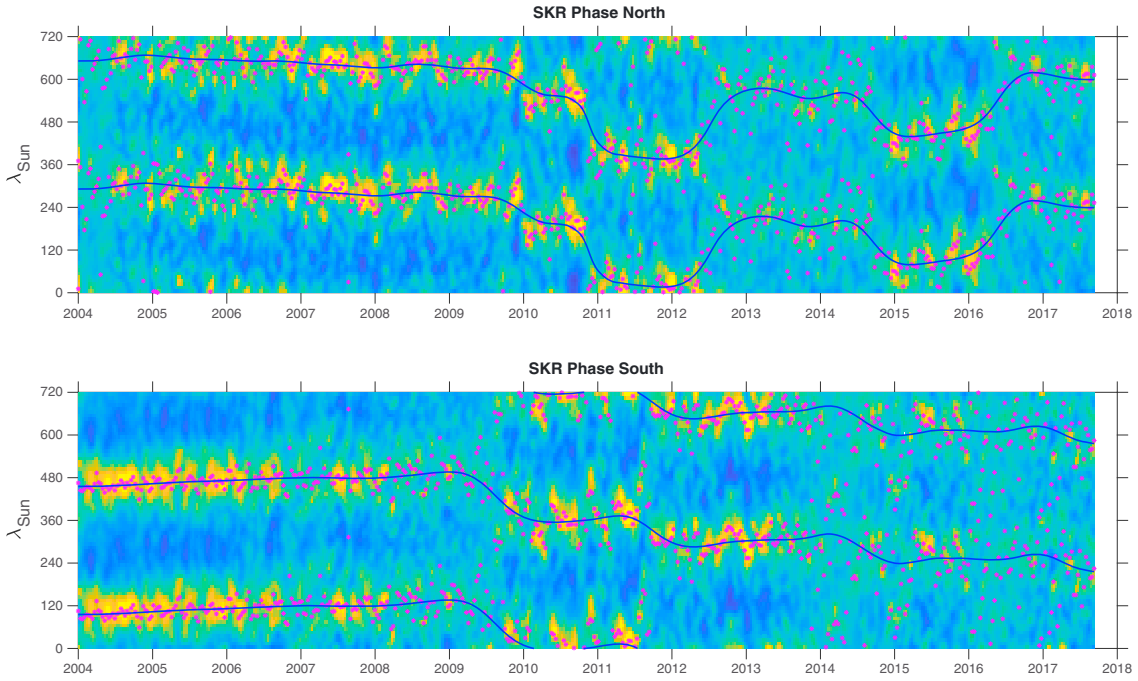

Figure 2. Zeroth-order phase diagram for (top panel) northern and (bottom panel) southern SKR plotted over two Saturn rotations as a function of year. The color of the spectrogram shows the SKR power normalized over each Saturn rotation, so that yellow indicates SKR peaks. The longitude λ_0 (vertical axis) is calculated by integrating the zeroth-order rotation rate from Figure 1 over time. The purple stars are directional statistics of the SKR phases, basically circular averages of subsolar longitudes weighted by normalized SKR power. The blue lines are smoothed values of the directional statistics.

The phase diagrams in Figure 2 show the normalized northern (top) and southern (bottom) SKR power as a function of the zeroth-order longitudes (different in the northern and southern hemispheres) and time. The color code is such that yellow indicates SKR peaks. The purple stars are directional statistics of the SKR phases, basically circular averages of subsolar longitudes weighted by normalized SKR power. The equations for the calculation of directional statistics are given in Appendix C of Fischer et al. (2015). The blue lines are smoothed values of the directional statistics. The slopes in the blue lines indicate phase drifts of SKR with respect to the zeroth-order longitude systems, which means that the zeroth-order rotation rates traced in Figure 1 are slightly off the true rotation rates. We correct the zeroth-order longitudes by subtracting the blue line values ($\Delta\varphi$) to get the SLS5 longitudes ($\lambda = \lambda_0 - \Delta\varphi$).

In Figure 3, the phase diagrams show the northern (top) and southern (bottom) SKR power as functions of the SLS5 subsolar longitudes and time. The northern and southern longitude systems are different because the rotation rates are different. The color code shows the SKR power normalized over each Saturn rotation, so that yellow indicates SKR peak intensity of each Saturn rotation. The SLS5 longitude (vertical axis) is calculated by subtracting the phase correction (blue line in Figure 2) from the zeroth-order longitude, which makes SKR peak around 0° subsolar longitudes in both northern and southern hemispheres, as shown by the yellow patches aligned along 0° longitude in Figure 3.

The rotation rates corresponding to the SLS5 longitude system can be derived by correcting the zeroth order rotation rates (ω_0) with the phase drift ($\Delta\varphi$) traced in Figure 2 ($\omega = \omega_0 - \frac{d\Delta\varphi}{dt}$). The corrected rotation rates for northern and southern SKR are shown as white solid lines in Figure 1, top and middle panels, respectively. It is shown that the correction with respect to the zeroth order rotation rates (white dotted lines) are minimal and the white lines still trace the rotation signals in the modulation spectrograms well.

The classical picture of SKR from the Voyager era assumed that SKR is modulated like a clock, which means that the timings of SKR intensifications is independent of the observer's local time and is better organized by subsolar longitude (Warwick et al., 1981). This picture has changed in the Cassini era in which two rotating current systems (one for each hemisphere) are thought to be linked to the creation of SKR in the upward current region (e.g., Andrews et al., 2011, and others). Lamy (2011) found SKR south emissions consistent with an

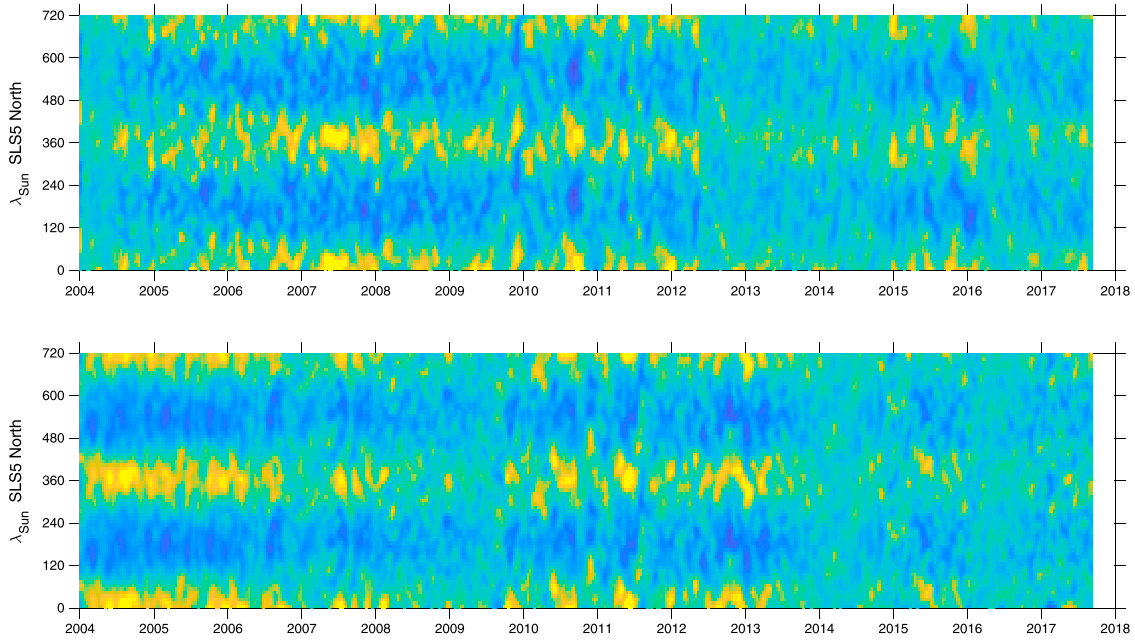

Figure 3. SLS5 phase diagram for (top panel) northern and (bottom panel) southern SKR plotted over two Saturn rotations as a function of year. The color of the spectrogram shows the SKR power normalized over each Saturn rotation, so that yellow indicates SKR peaks. The SLS5 longitude (vertical axis) is calculated by subtracting the phase correction (blue line in Figure 2) from the zeroth-order longitude so that SKR peak around 0° SLS5 longitudes in both northern and southern hemispheres.

intrinsically rotating phenomena, which is also linked to UV emissions from the aurora (Lamy et al., 2013). However, the dominance of the SKR morning side sources leads to a clock-like appearance of SKR in certain local time regions. The model of Andrews et al. (2011, their Figure 2, and see the right panel of our Figure 4) shows a clock-like behavior in the local time region of 4 hr to noon (dawnside, zero SKR phase deviation $\Delta\varphi_{LT}$) and a rotating signal from noon to 4 hr over the duskside with a changing SKR phase deviation. Due to the mostly eccentric Cassini orbits the SKR phase deviations were generally dominated by the observations near apoapsis where the spacecraft spent most time. Since the local time change of the spacecraft was small around apoapsis, the SKR actually *appeared* clock-like, and a distinction between clock-like and rotating signals can in principle only be done when the spacecraft quickly traverses over a large region in local time (i.e., around periapsis; Wang et al., 2010). So for a single elliptical orbit with high eccentricity large changes in the SKR phase deviation $\Delta\varphi_{LT}$ will only occur for a few days around periapsis, but Cassini orbits usually lasted a few weeks, and the period determination for SKR employs sliding windows of several months. So what is relevant is not the SKR phase change within a single orbit, but it is the progression of the local time of Cassini apoapsis over the years. To take this effect into account Andrews et al. (2011) defined the so-called orbit-averaged SKR phase deviation $\overline{\Delta\varphi_{LT}}$, where a single value for the SKR phase deviation is calculated for each orbit. We have calculated the orbit-averaged SKR phase deviations from 2004 until the end of the Cassini mission in a similar way as Andrews et al. (2011) by calculating the directional mean of all phase deviations in 10-min intervals from one apoapsis pass to the next (with 1 January 2004 as the starting point and the end of mission on 15 September 2017 as the end point). The result can be seen in the left panel of Figure 4. The right panel shows that most orbit-averaged SKR phase deviations follow the model of Andrews et al. (2011), indicated by the black line, well. A few orbits (red stars in Figure 4) deviate from the model due to their small eccentricity, and such almost circular orbits occurred around large local time shifts of Cassini apoapsis.

The orbit-averaged SKR phase deviation $\overline{\Delta\varphi_{LT}}$ can now be used to construct a true strobe phase Φ_{SKR}* with the equation $\Phi^*_{SKR}(t) = \Phi_{SKR}(t) + \overline{\Delta\varphi_{LT}}(t)$ (equation (3d) of Andrews et al. (2011)), with Φ_{SKR} as the observed SKR phase with the maxima around 0° as shown in Figure 3. This additional phase correction now leads us from the SLS5 system to an SLS5* system, which takes the spacecraft position into account. When Cassini apoapsis is at the afternoon side the SLS5* longitude is larger than the SLS5 longitude ($\overline{\Delta\varphi_{LT}} > 0$), since a hypothetical

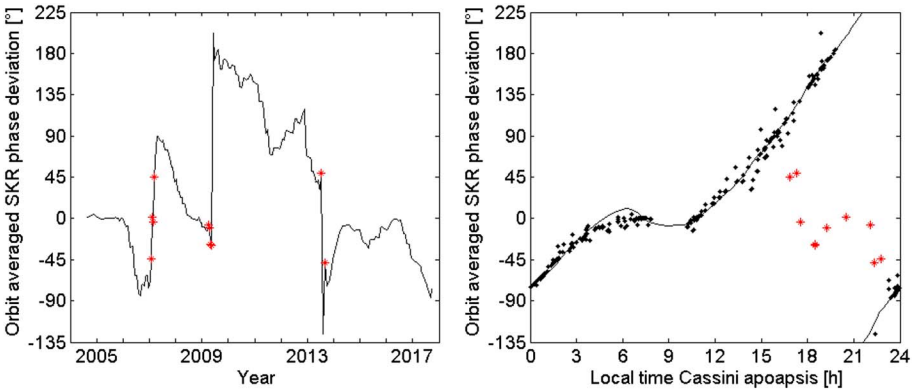

Figure 4. The left panel shows the orbit-averaged SKR phase deviation from 2004 until the end of the Cassini mission as a function of time. The right panel shows the orbit-averaged phase deviations as a function of the local times of Cassini apoapsis passes for each Cassini orbit. The black line indicates the model of Andrews et al. (2011), and most orbits follow the model except 10 orbits indicated by red stars in both panels.

spacecraft on the morning side would have seen the SKR maximum earlier than a spacecraft on the afternoon side, and therefore, the SLS5* value must have already progressed by the time the maximum is observed by the spacecraft on the afternoon side. It is vice versa for a spacecraft around midnight ($\overline{\Delta\varphi_{LT}} < 0$). The SLS5* system can thus be understood as the SKR phase observed by a hypothetical spacecraft at a constant local time position on the morning side where the SKR phase deviation is zero (e.g., around 7.3 LT). The SLS5 system reflects the SKR phases as they were really observed by Cassini.

The SLS5* system is based on the model of Andrews et al. (2011), which might undergo modifications in future, and therefore, we provide both systems to the scientific community. The model of Andrews et al. (2011) is based on an SKR seeing function of a 1 hr broad local time window centered at ±55° (±3.7 LT) around the local time position of the spacecraft. This assumption might be a good first approximation, but it has been shown that SKR beaming angles vary from 55° to 80° and also depend on frequency (Cecconi et al., 2009). The seeing function probably depends on the observer's latitude since an observer at high latitude might also see phase-shifted radio sources from the farside of the auroral oval. We also emphasize to use the SLS5* system with care at Cassini orbits with low eccentricity, especially from mid-January to early April 2007, from late March to early June 2009, and from early July to mid-September 2013 (red stars in Figure 4). The SLS5* system is given with the same temporal resolution as the SLS5 system, which is one value every 10 min. The calculation of the orbit-averaged SKR phase deviation gives just one value per orbit. We put these values roughly into the middle of the respective interval (at the periapsis times) and made simple linear interpolations between them.

2. Discussion

We have defined a new longitude system for Saturn based on the rotational modulation of SKR observed during the Cassini mission. The SLS5 system is defined such that the north/south SKR power observed by Cassini peaks at 0° longitude. The SLS5* system is defined as the SKR phase that would have been observed by a hypothetical spacecraft on the morning side, where the main source of SKR would always be visible. The system is valid from 1 January 2004 to the end of the mission, 15 September 2017. The north and south subsolar longitude values for every 10-min interval can be accessed as a text file in the supporting information. For other times, the longitude values can be interpolated from the provided values. The longitude of the spacecraft can be derived from the subsolar longitudes as $\lambda_{SC} = \lambda_{Sun} + (12 - LT_{SC}) \times 15^{\circ}$.

Figure S1 compares SLS4 and SLS5 subsolar longitudes for the northern (top) and southern (bottom) hemispheres for the two-day period between 5 and 7 February 2009. It is shown that the two systems agree with each other quite well. The difference between the SLS4 and SLS5 longitudes is about 10° and 40° in the northern and southern hemispheres, respectively. Similar comparisons for other periods revealed that the difference varies over time. In Figure S2, we plot the difference between the two systems over time, from 2004 to 2010. It is shown that the difference between the SLS4 and SLS5 subsolar longitudes remains close

to zero for most of the period in which both systems are defined, except in 2009 when the difference increases with time. The solid blue areas (periodic oscillations between −180° and 180°) are due to the SLS4 longitudes being set to zero when SLS4 is not defined. The fast variation of the difference between SLS4 and SLS5 longitudes in 2009 is almost certainly due to the different SKR modulation rates determined by Gurnett et al. (2011) and this study.

Gurnett et al. (2011) used a tracking filter analysis method to enhance the signal-to-noise level of the modulation signal in 2009, when the rotation rates were changing quickly (their Figure 6). They used total SKR power and assumed that the north rate is faster than the south rate. So the tracking filter analysis was carried out separately for two hemispheres and the spectra were merged at an intermediate frequency of the north and south components. The spectrograms in Figure 1, however, are created from SKR powers separated in hemisphere by latitude/polarization, and the LSSA does not take into account the rapid change of the rotation rates around equinox. The LSSA spectrograms show that, in late 2009, the north rate slowed rapidly from ~812 to ~805°/day and the south rate increased rapidly from ~803 to 810°/day, indicating that the two rotation rates switched right after equinox. This is consistent with the SKR modulation analysis presented by Fischer et al. (2015) and Ye et al. (2016). The discrepancy between Gurnett et al. (2011) and later studies' identification of rotation rates is due to the low signal-to-noise ratio in SKR's modulation in 2009, most likely caused by the rapid variation of the rotation rates due to the seasonal variation in Saturn's polar regions (Gurnett et al., 2010). The low signal-to-noise level for the postequinox periods can also be identified in the phase diagrams in Figure 3, where the yellow bands formed by the SKR intensity peaks are not as evident as the periods when SKR modulation signals are strong.

3. Summary

Saturn's radio emissions and many other phenomena observed by instruments onboard Cassini are modulated at similar periods close to the planet's rotation period. Two components have been found in the rotational modulation of Saturn's radio emissions and other phenomena, one associated with the northern hemisphere and the other associated with the southern hemisphere. The two components have also been found to display seasonal variation, most likely due to the different solar illumination on the two polar regions, where the dynamics in the upper level atmosphere could couple with the magnetosphere through field-aligned currents (Jia et al., 2012; Jia & Kivelson, 2012; Smith, 2006, 2014, 2018; Smith et al., 2016; Southwood & Cowley, 2014). RPWS provided the most continuous measurements of the rotation periods in the two hemispheres, which have been shown to be generally consistent with the modulation periods measured by other instruments when simultaneous observations are available (Carbary, 2017; Cowley & Provan, 2016). Using a LSSA and a phase tracing method, we defined a new longitude system (SLS5) based on the modulation phase of SKR. The SLS5 system organizes the observed north/south SKR maxima around 0° longitude. Based on a simple visibility model given by Andrews et al. (2011), assuming on the dusk side Cassini only saw a rotating SKR source, we also calculated the north/south SKR phases that would have been observed if the main source on the morning side were always visible, the SLS5* longitudes. The new longitude system can be used to organize other magnetospheric events such as hot plasma injections, similar to the study carried out by Kennelly et al. (2013). The longitude values for the northern and southern hemispheres in 10-min intervals can be accessed in the supporting information of this paper.

Acknowledgments
This research was supported by NASA through contract 1415150 with the Jet Propulsion Laboratory. The data used in this study are available through the Planetary Data System or from the authors. The paper also benefited from the discussions in the international team workshop "Rotational phenomena in Saturn's magnetosphere" funded by the International Space Science Institute (ISSI) in Bern, Switzerland. We thank Laurent Lamy for helpful discussions regarding SKR modulations toward the end of the Cassini mission and Baptiste Cecconi for providing the level 3 HFR data we used in this study.

References

Andrews, D. J., Bunce, E. J., Cowley, S. W. H., Dougherty, M. K., Provan, G., & Southwood, D. J. (2008). Planetary period oscillations in Saturn's magnetosphere: Phase relation of equatorial magnetic field oscillations and Saturn kilometric radiation modulation. *Journal of Geophysical Research*, *113*, A09205. https://doi.org/10.1029/2007JA012937

Andrews, D. J., Cecconi, B., Cowley, S. W. H., Dougherty, M. K., Lamy, L., Provan, G., & Zarka, P. (2011). Planetary period oscillations in Saturn's magnetosphere: Evidence in magnetic field phase data for rotational modulation of Saturn kilometric radiation emissions. *Journal of Geophysical Research*, *116*, A09206. https://doi.org/10.1029/2011JA016636

Andrews, D. J., Coates, A. J., Cowley, S. W. H., Dougherty, M. K., Lamy, L., Provan, G., & Zarka, P. (2010). Magnetospheric period oscillations at Saturn: Comparison of equatorial and high-latitude magnetic field periods with north and south Saturn kilometric radiation periods. *Journal of Geophysical Research*, *115*, A12252. https://doi.org/10.1029/2010JA015666

Andrews, D. J., Cowley, S. W. H., Dougherty, M. K., Lamy, L., Provan, G., & Southwood, D. J. (2012). Planetary period oscillations in Saturn's magnetosphere: Evolution of magnetic oscillation properties from southern summer to post-equinox. *Journal of Geophysical Research*, *117*, A04224. https://doi.org/10.1029/2011JA017444

Andrews, D. J., Cowley, S. W. H., Dougherty, M. K., & Provan, G. (2010). Magnetic field oscillations near the planetary period in Saturn's equatorial magnetosphere: Variation of amplitude and phase with radial distance and local time. *Journal of Geophysical Research*, *115*, A04212. https://doi.org/10.1029/2009JA014729

Burton, M. E., Dougherty, M. K., & Russell, C. T. (2010). Saturn's internal planetary magnetic field. *Geophysical Research Letters*, *37*, L24105. https://doi.org/10.1029/2010GL045148

Carbary, J. F. (2017). Update on Saturn's energetic electron periodicities. *Journal of Geophysical Research: Space Physics*, *122*, 156–165. https://doi.org/10.1002/2016JA023405

Carbary, J. F., & Mitchell, D. G. (2013). Periodicities in Saturn's magnetosphere. *Reviews of Geophysics*, *51*(1), 1–30. https://doi.org/10.1002/rog.20006

Carbary, J. F., Mitchell, D. G., Kollmann, P., Krupp, N., & Roussos, E. (2017). Energetic electron periodicities during the Cassini grand finale. *Journal of Geophysical Research: Space Physics*, *122*, 12,229–12,235. https://doi.org/10.1002/2017JA024836

Carbary, J. F., Mitchell, D. G., Krimigis, S. M., Hamilton, D. C., & Krupp, N. (2007). Charged particle periodicities in Saturn's outer magnetosphere. *Journal of Geophysical Research*, *112*, A06246. https://doi.org/10.1029/2007JA012351

Cecconi, B., Lamy, L., Zarka, P., Prange, R., Kurth, W. S., & Louarn, P. (2009). Goniopolarimetric study of the revolution 29 perikrone using the Cassini Radio and Plasma Wave Science instrument high-frequency radio receiver. *Journal of Geophysical Research*, *114*, A03215. https://doi.org/10.1029/2008JA013830

Cecconi, B., & Zarka, P. (2005). Direction finding and antenna calibration through analytical inversion of radio measurements performed using a system of two or three electric dipole antennas on a three-axis stabilized spacecraft. *Radio Science*, *40*, RS3003. https://doi.org/10.1029/2004RS003070

Clarke, K. E., Andrews, D. J., Arridge, C. S., Coates, A. J., & Cowley, S. W. H. (2010). Magnetopause oscillations near the planetary period at Saturn: Occurrence, phase, and amplitude. *Journal of Geophysical Research*, *115*, A08209. https://doi.org/10.1029/2009JA014745

Clarke, K. E., Andrews, D. J., Coates, A. J., Cowley, S. W. H., & Masters, A. (2010). Magnetospheric period oscillations of Saturn's bow shock. *Journal of Geophysical Research*, *115*, A05202. https://doi.org/10.1029/2009JA015164

Cowley, S. W. H., & Provan, G. (2016). Planetary period oscillations in Saturn's magnetosphere: Further comments on the relation between post-equinox properties deduced from magnetic field and Saturn kilometric radiation measurements. *Icarus*, *272*, 258–276. https://doi.org/10.1016/j.icarus.2016.02.051

Davies, M. E., Abalakin, V. K., Bursa, M., Lieske, J. H., Morando, B., Morrison, D., et al. (1996). Report of the IAU/COSPAR working group on cartographic coordinates and rotational elements of the planets and satellites. *Celestial Mechanics and Dynamical Astronomy*, *63*, 127–148.

Desch, M. D., & Kaiser, M. L. (1981). Voyager measurement of the rotation period of Saturn's magnetic field. *Geophysical Research Letters*, *8*(3), 253–256. https://doi.org/10.1029/GL008i003p00253

Espinosa, S. A., & Dougherty, M. K. (2000). Periodic perturbations in Saturn's magnetic field. *Geophysical Research Letters*, *27*(17), 2785–2788. https://doi.org/10.1029/2000GL000048

Espinosa, S. A., Southwood, D. J., & Dougherty, M. K. (2003). How can Saturn impose its rotation period in a noncorotating magnetosphere? *Journal of Geophysical Research*, *108*(A2), 1086. https://doi.org/10.1029/2001JA005084

Fischer, G., Cecconi, B., Lamy, L., Ye, S. Y., Taubenschuss, U., Macher, W., et al. (2009). Elliptical polarization of Saturn kilometric radiation observed from high latitudes. *Journal of Geophysical Research*, *114*, A08216. https://doi.org/10.1029/2009JA014176

Fischer, G., Gurnett, D. A., Kurth, W. S., Ye, S. Y., & Groene, J. B. (2015). Saturn kilometric radiation periodicity after equinox. *Icarus*, *254*, 72–91. https://doi.org/10.1016/j.icarus.2015.03.014

Fischer, G., Ye, S. Y., Groene, J. B., Ingersoll, A. P., Sayanagi, K. M., Menietti, J. D., et al. (2014). A possible influence of the Great White Spot on Saturn kilometric radiation periodicity. *Annales Geophysicae*, *32*(12), 1463–1476. https://doi.org/10.5194/angeo-32-1463-2014

Galopeau, P. H., & Lecacheux, A. (2000). Variations of Saturn's radio rotation period measured at kilometer wavelengths. *Journal of Geophysical Research*, *105*(A6), 13,089–13,101. https://doi.org/10.1029/1999JA005089

Gurnett, D. A., Groene, J. B., Averkamp, T. F., Kurth, W. S., Ye, S. Y., & Fischer, G. (2011). An SLS4 longitude system based on a tracking filter analysis of the rotational modulation of Saturn kilometric radiation. In *Planetary radio emissions VII* (pp. 51–64). Vienna, Austria: Austrian Academy of Sciences Press.

Gurnett, D. A., Groene, J. B., Persoon, A. M., Menietti, J. D., Ye, S. Y., Kurth, W. S., et al. (2010). The reversal of the rotational modulation rates of the north and south components of Saturn kilometric radiation near equinox. *Geophysical Research Letters*, *37*, L24101. https://doi.org/10.1029/2010GL045796

Gurnett, D. A., Kurth, W. S., Hospodarsky, G. B., Persoon, A. M., Averkamp, T. F., Cecconi, B., et al. (2005). Radio and plasma wave observations at Saturn from Cassini's approach and first orbit. *Science*, *307*(5713), 1255–1259. https://doi.org/10.1126/science.1105356

Gurnett, D. A., Lecacheux, A., Kurth, W. S., Persoon, A. M., Groene, J. B., Lamy, L., et al. (2009). Discovery of a north-south asymmetry in Saturn's radio rotation period. *Geophysical Research Letters*, *36*, L16102. https://doi.org/10.1029/2009GL039621

Gurnett, D. A., Persoon, A. M., Groene, J. B., Kopf, A. J., Hospodarsky, G. B., & Kurth, W. S. (2009). A north-south difference in the rotation rate of auroral hiss at Saturn: Comparison to Saturn's kilometric radio emission. *Geophysical Research Letters*, *36*, L21108. https://doi.org/10.1029/2009GL040774

Gurnett, D. A., Persoon, A. M., Kurth, W. S., Groene, J. B., Averkamp, T. F., Dougherty, M. K., & Southwood, D. J. (2007). The variable rotation period of the inner region of Saturn's plasma disk. *Science*, *316*(5823), 442–445. https://doi.org/10.1126/science.1138562

Hunt, G. J., Cowley, S. W. H., Provan, G., Bunce, E. J., Alexeev, I. I., Belenkaya, E. S., et al. (2014). Field-aligned currents in Saturn's southern nightside magnetosphere: Subcorotation and planetary period oscillation components. *Journal of Geophysical Research: Space Physics*, *119*, 9847–9899. https://doi.org/10.1002/2014JA020506

Hunt, G. J., Cowley, S. W. H., Provan, G., Bunce, E. J., Alexeev, I. I., Belenkaya, E. S., et al. (2015). Field-aligned currents in Saturn's northern nightside magnetosphere: Evidence for interhemispheric current flow associated with planetary period oscillations. *Journal of Geophysical Research: Space Physics*, *120*, 7552–7584. https://doi.org/10.1002/2015JA021454

Jia, X., & Kivelson, M. G. (2012). Driving Saturn's magnetospheric periodicities from the upper atmosphere/ionosphere: Magnetotail response to dual sources. *Journal of Geophysical Research*, *117*, A11219. https://doi.org/10.1029/2012JA018183

Jia, X., Kivelson, M. G., & Gombosi, T. I. (2012). Driving Saturn's magnetospheric periodicities from the upper atmosphere/ionosphere. *Journal of Geophysical Research*, *117*, A04215. https://doi.org/10.1029/2012JA018183

Kennelly, T. J., Leisner, J. S., Hospodarsky, G. B., & Gurnett, D. A. (2013). Ordering of injection events within Saturnian SLS longitude and local time. *Journal of Geophysical Research: Space Physics*, *118*, 832–838. https://doi.org/10.1002/jgra.50152

Khurana, K. K., Mitchell, D. G., Arridge, C. S., Dougherty, M. K., Russell, C. T., Paranicas, C., et al. (2009). Sources of rotational signals in Saturn's magnetosphere. *Journal of Geophysical Research*, *114*, A02211. https://doi.org/10.1029/2008JA013312

Kurth, W. S., Averkamp, T. F., Gurnett, D. A., Groene, J. B., & Lecacheux, A. (2008). An update to a Saturnian longitude system based on kilometric radio emissions. *Journal of Geophysical Research*, *113*, A05222. https://doi.org/10.1029/2007JA012861

Kurth, W. S., Lecacheux, A., Averkamp, T. F., Groene, J. B., & Gurnett, D. A. (2007). A Saturnian longitude system based on a variable kilometric radiation period. *Geophysical Research Letters*, *34*, L02201. https://doi.org/10.1029/2007JA012861

Lamy, L. (2011). Variability of Southern and Northern Saturn Kilometric Radiation Periodicities. In *Planetary Radio Emissions VII* (pp. 39–50). Vienna, Austria: Austrian Academy of Sciences Press.

Lamy, L. (2017). The Saturnian Kilometric Radiation before the Cassini Grand Finale. In G. Fischer, G. Mann, M. Panchenko, & P. Zarka (Eds.), *Planetary radio emissions VIII* (pp. 171–190). Vienna: Austrian Academy of Sciences Press.

Lamy, L., Prangé, R., Pryor, W., Badman, S. V., Melin, H., Stallard, T., et al. (2013). Multispectral simulataneous diagnosis of Saturn's aurorae throughout a planetary rotation. *Journal of Geophysical Research: Space Physics*, *118*, 4817–4843. https://doi.org/10.1002/jgra.50404

Lamy, L., Schippers, P., Zarka, P., Cecconi, B., Arridge, C. S., Dougherty, M. K., et al. (2010). Properties of Saturn kilometric radiation measured within its source region. *Geophysical Research Letters*, *37*, L12104. https://doi.org/10.1029/2010GL043415

Lecacheux, A., Galopeau, P., & Aubier, M. (1997). Re-visiting Saturnian kilometric radiation with Ulysses/URAP. In *Planetary radio emissions IV* (pp. 313–325). Vienna, Austria: Austrian Academy of Sciences Press.

Lomb, N. R. (1976). Least-squares frequency analysis of unequally spaced data. *Astrophysics and Space Science*, *39*(2), 447–462. https://doi.org/10.1007/BF00648343

Menietti, J. D., Mutel, R. L., Schippers, P., Ye, S. Y., Gurnett, D. A., & Lamy, L. (2011). Analysis of Saturn kilometric radiation near a source center. *Journal of Geophysical Research*, *116*, A12222. https://doi.org/10.1029/2011JA017056

Nichols, J. D., Cecconi, B., Clarke, J. T., Cowley, S. W. H., Gérard, J. C., Grocott, A., et al. (2010). Variation of Saturn's UV aurora with SKR phase. *Geophysical Research Letters*, *37*, L15102. https://doi.org/10.1029/2010GL044057

Paranicas, C., Mitchell, D. G., Roelof, E. C., Brandt, P. C., Williams, D. J., Krimigis, S. M., & Mauk, B. H. (2005). Periodic intensity variations in global ENA images of Saturn. *Geophysical Research Letters*, *32*, L21101. https://doi.org/10.1029/2005GL023656

Priestly, M. B. (1981). *Spectral analysis and time series* (Vol. 443). London: Academic Press.

Provan, G., Andrews, D. J., Arridge, C. S., Coates, A. J., Cowley, S. W. H., Milan, S. E., et al. (2009). Polarization and phase of planetary-period magnetic field oscillations on high-latitude field lines in Saturn's magnetosphere. *Journal of Geophysical Research*, *114*, A02225. https://doi.org/10.1029/2008JA013782

Provan, G., Andrews, D. J., Cecconi, B., Cowley, S. W. H., Dougherty, M. K., Lamy, L., & Zarka, P. (2011). Magnetospheric period magnetic field oscillations at Saturn: Equatorial phase "jitter" produced by superposition of southern and northern period oscillations. *Journal of Geophysical Research*, *116*, A04225. https://doi.org/10.1029/2010JA016213

Provan, G., Cowley, S. W. H., Bradley, T. J., Bunce, E. J., Hunt, G. J., & Dougherty, M. K. (2018). Planetary Period Oscillations in Saturn's Magnetosphere: Cassini Magnetic Field Observations Over the Northern Summer Solstice Interval. *Journal of Geophysical Research: Space Physics*, *123*, 3859–3899. https://doi.org/10.1029/2018JA025237

Provan, G., Lamy, L., Cowley, S. W., & Dougherty, M. K. (2014). Planetary period oscillations in Saturn's magnetosphere: Comparison of magnetic oscillations and SKR modulations in the postequinox interval. *Journal of Geophysical Research: Space Physics*, *119*, 7380–7401. https://doi.org/10.1002/2014JA020011

Provan, G., Tao, C., Cowley, S. W. H., Dougherty, M. K., & Coates, A. J. (2015). Planetary period oscillations in Saturn's magnetosphere: Examining the relationship between abrupt changes in behavior and solar wind-induced magnetospheric compressions and expansions. *Journal of Geophysical Research: Space Physics*, *120*, 9524–9544. https://doi.org/10.1002/2015JA021642

Scargle, J. D., 1982. "Studies in astronomical time series analysis. II—Statistical aspects of spectral analysis of unevenly spaced data". *Astrophysical Journal*. *263*, 835-853. https://doi.org/10.1086/160554

Seidelmann, P. K., Abalakin, V. K., Bursa, M., Davies, M. E., de Bergh, C., Lieske, J. H., et al. (2002). Report of the IAU/IAG working group on cartographic coordinates and rotational elements of the planets and satellites:2000. *Celestial Mechanics and Dynamical Astronomy*, *82*, 83–110.

Smith, C. G. A. (2006). Periodic modulation of gas giant magnetospheres by the neutral upper atmosphere. *Annales Geophysicae*, *24*(10), 2709–2717.

Smith, C. G. A. (2014). On the nature and location of the proposed twin vortex systems in Saturn's polar upper atmosphere. *Journal of Geophysical Research: Space Physics*, *119*, 5964–5977. https://doi.org/10.1002/2014JA019934

Smith, C. G. A. (2018). Interaction of Saturn's dual rotation periods. *Icarus*, *302*, 330–342.

Smith, C. G. A., Ray, L. C., & Achilleos, N. A. (2016). A planetary wave model for Saturn's 10.7-h periodicities. *Icarus*, *268*, 76–88.

Southwood, D. J., & Cowley, S. W. H. (2014). The origin of Saturn's magnetic periodicities: Northern and southern current systems. *Journal of Geophysical Research: Space Physics*, *119*, 1563–1571. https://doi.org/10.1002/2013JA019632

Wang, Z., Gurnett, D. A., Fischer, G., Ye, S. Y., Kurth, W. S., Mitchell, D. G., et al. (2010). Cassini observations of narrowband radio emissions in Saturn's magnetosphere. *Journal of Geophysical Research*, *115*, A06213. https://doi.org/10.1029/2009JA014847

Warwick, J. W., Pearce, J. B., Evans, D. R., Carr, T. D., Schauble, J. J., Alexander, J. K., et al. (1981). Planetary radio astronomy observations from Voyager 1 near Saturn. *Science*, *212*(4491), 239–243.

Wu, C. S., & Lee, L. C. (1979). A theory of the terrestrial kilometric radiation. *The Astrophysical Journal*, *230*, 621–626.

Ye, S. Y., Fischer, G., Kurth, W. S., Menietti, J. D., & Gurnett, D. A. (2016). Rotational modulation of Saturn's radio emissions after equinox. *Journal of Geophysical Research: Space Physics*, *121*, 11,714–11,728. https://doi.org/10.1002/2016JA023281

Ye, S. Y., Gurnett, D. A., Groene, J. B., Wang, Z., & Kurth, W. S. (2010). Dual periodicities in the rotational modulation of Saturn narrowband emissions. *Journal of Geophysical Research*, *115*, A12258. https://doi.org/10.1029/2010JA015780

Erratum

In the originally published version of this article, section 1.1 concluded with the following sentence, which has since been deleted: "However, no new longitude system was defined due to the difficulty in determining the north and south SKR periods after Saturn's vernal equinox, especially 2010–2012." The present version may be considered the authoritative version of record.